16th World Congress in Computational Mechanics (WCCM)
21-26 July 2024, Vancouver, Canada
A. Korobenko, M. Laforest, S. Prudhomme, R. Vaziri (Eds)

BAND GAP EVOLUTION IN NONLINEAR DYNAMICS OF METAMATERIALS MADE STRUCTURES VIA GRADUALLY-CHANGING MECHANICAL PROPERTIES

R. Augello[1], **E. Carrera**[1,2]

[1] Mul[2] Group
Department of Mechanical and Aerospace Engineering, Politecnico di Torino
Corso Duca degli Abruzzi 24, 10129 Torino, Italy
riccardo.augello@polito.it

[2] Department of Mechanical Engineering, College of Engineering
Prince Mohammad Bin Fahd University P.O. Box 1664. Al Khobar 31952
Kingdom of Saudi Arabia
erasmo.carrera@polito.it

Key words: Metamaterial, Band-gap evolution, FEM, Carrera unified formulation.

Abstract. This paper explores the dynamic behavior of metamaterial-like structures by investigating the evolution of their band gap under the influence of geometrical nonlinearities in the large displacement/rotations field. The study employs a unified framework based on the Carrera Unified Formulation (CUF) and a total Lagrangian approach to develop higher-order one-dimensional beam theories that account for geometric nonlinearities. The axis discretization is achieved through a finite element approximation. The equations of motion are solved around nonlinear static equilibrium states, which are determined using a Newton–Raphson algorithm combined with a path-following method of arc-length type. The CUF approach introduces two key innovations that are highly suitable for the evolution of the band gap:
1) Thin-walled structures can be effectively represented using a **single** one-dimensional beam model, overcoming the common limitations of standard finite elements. This is crucial as three-dimensional solid elements would result in significant computational costs, and two-dimensional elements pose limitations for this type of investigation. Finally, employing one-dimensional finite elements usually requires a combination of elements, leading to additional mathematical complexities in their connections and lacking geometric precision.
2) CUF enables the use of the full Green-Lagrange strain tensor without the need for assumptions, as is the case with von Kármán nonlinearities.
The paper specifically compares results obtained with linear and nonlinear stiffness matrices, highlighting the differences. Numerical investigations are conducted on thin-walled structures composed of repeatable cells, assessing mode changes under traction and compression loading. The findings emphasize that the band gap is an inherent property of the equilibrium state, underscoring the necessity of a proper nonlinear analysis for accurately evaluating frequency transitions.

1 Introduction

Metamaterials stand out due to their unique properties that differ from those found in nature, providing unmatched control over wave propagation in both electromagnetic and acoustic fields. Unlike conventional materials, which are constrained by natural properties and exhibit predictable behaviors, metamaterials allow designers to tailor responses to specific inputs. The band gap plays a crucial role in determining how metamaterials interact with and control waves, presenting exceptional opportunities for customization in various applications.
An essential part of designing the band gaps and structural behavior of metamaterials is numerical simulation. Traditional methods typically rely on three-dimensional (3D) and two-dimensional (2D) simulations, which face challenges due to high computational costs and significant nonlinear approximations, respectively. This study presents a solution involving the application of the Carrera Unified Formulation (CUF) [1, 2]. CUF offers two significant advancements ideal for metamaterials analysis: the capability to efficiently represent them using a singular one-dimensional (1D) beam model and the incorporation of the complete Green-Lagrange strain tensor. The first innovation addresses the typical constraints of standard finite element methods, significantly reducing the computational cost associated with solid finite elements and surpassing the limitations of both 2D and 1D models. The second key feature effectively overcomes nonlinear assumptions, particularly in scenarios involving von Kármán nonlinearities, as seen in 2D elements. Moreover, the proposed approach allows for the implementation of any nonlinear assumption to evaluate the accuracy and reliability of different theories.
The research delves into the examination of thin-walled structures and metamaterials, emphasizing the alteration of band gap characteristics as these materials undergo significant displacement and changes in mechanical properties. This study extends to include a comprehensive nonlinear analysis, integrating the complete Green-Lagrange strain equations, which is critical for accurately assessing the behavior of these materials. Practical examples are provided to illustrate the evolution and development of band gaps in these structures. A key aspect of this research is the comparison of results obtained from this comprehensive approach with those derived from von Kármán approximations. This comparative analysis highlights the enhanced accuracy and relevance of incorporating full Green-Lagrange strains in understanding the dynamic properties of thin-walled and metamaterial structures.

2 Refined one-dimensional finite element

The three-dimensional (3D) displacement field of a generic one-dimensional (1D) beam structure can be written in a vectorial form, and it reads:

$$\mathbf{u}(x, y, z) = \{u_x \; u_y \; u_z\}^T \tag{1}$$

where x, y and z are the coordinates of a Cartesian reference system. Assume that y is the direction of the beam axis, whereas x and z are the coordinates of the cross-section. The Carrera Unified Formulation (CUF) and the Finite Element Method (FEM) allows the 3D displacement

field to be expressed as follows:

$$\mathbf{u}(x,y,z) = F_\tau(x,z)N_i(y)\mathbf{u}_{\tau i} \qquad \tau = 1,2,...,M \qquad i = 1,2,\ldots,N_n \tag{2}$$

where $F_\tau(x,z)$ are the cross-section expansion functions in the x and z directions, where N_i stands for the ith shape function in the y direction, M represents the number of the terms used in the expansion, N_n stands for the number of the nodes on the beam axis and $\mathbf{u}_{\tau i}$ is the vector of the nodal unknowns. Lagrange Expansions (LE) are used as cross-sectional functions. They can ensure linear (L4), quadratic (L9), and cubic interpolation (L16), allowing the implementation of linear to higher-order kinematics. Carrera and Petrolo [3] provided more details about LE beam theories.

Let us consider a thin-walled structure made of repeatable cells. Three types of modeling are ensured by commercial software. Figure 1 shows them, i.e. the use of 3D, 2D and 1D Finite Elements (FEs). While the former stands out as the most accurate solution, it falls short in

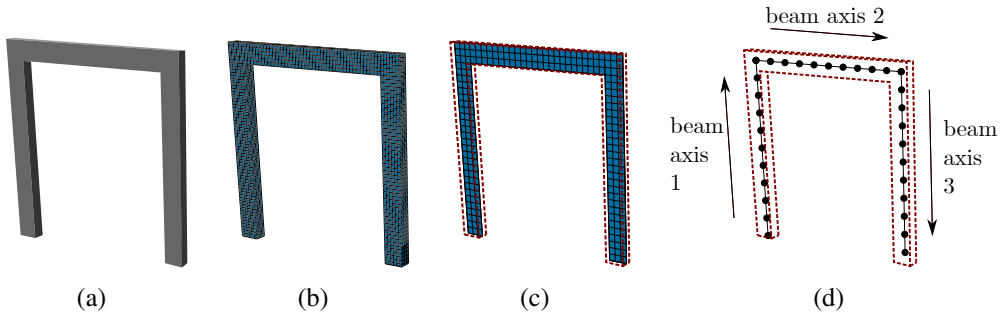

Figure 1: Different approaches for the thin-walled structure made of repeatable cells (a), i.e. the use of 3D (b), 2D (c) and 1D (d)FEs.

terms of computational efficiency. As emphasized in [4], a reliable through-thickness analysis requires the utilization of at least three to four solid elements. The thin nature of the components, coupled with the aspect ratio constraints inherent in 3D Finite Elements (FEs), results in a substantial number of degrees of freedom. Conversely, while opting for 2D Finite Elements (FEs) may seem reasonable given the slim profile of the structure, these elements lack the capacity to capture through-thickness strain and stress components, which can be pivotal from a design perspective. Similar conclusions apply to the final modeling approach involving 1D FEs. In this scenario, the structure is represented as multiple beams, typically relying on classical theories within commercial software. However, the drawbacks of classical theories, such as the omission of shear strain and lack of geometric exactitude, persist in this modeling technique. Figure 2 shows the proposed mathematical modeling approach based on CUF. In this instance, the structure is represented as a single beam. As illustrated in Fig. 2, the cross-section of the beam lies in the plane $x-z$ and is delineated in red, while the beam axis, depicted in blue, aligns with the y direction. The discretization of the cross-section is achieved using high-order Lagrange polynomials, enabling the accurate depiction of both local and global deformations

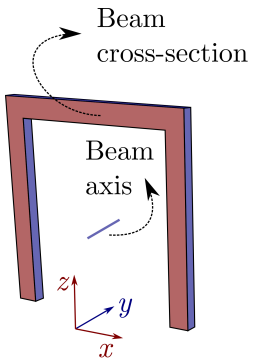

Figure 2: Proposed mathematical modeling approach based on CUF.

and providing an exact representation of the geometry. With this approach, displacement continuity between elements and sudden geometric changes are automatically ensured by the shared Lagrange points.

2.1 Geometrical and constitutive relations

The stress, σ, and strain, ϵ, components are expressed in vectorial form with no loss of generality,

$$\begin{aligned} \sigma &= \{\sigma_{xx} \quad \sigma_{yy} \quad \sigma_{zz} \quad \sigma_{xz} \quad \sigma_{yz} \quad \sigma_{xy}\}^T \\ \epsilon &= \{\epsilon_{xx} \quad \epsilon_{yy} \quad \epsilon_{zz} \quad \epsilon_{xz} \quad \epsilon_{yz} \quad \epsilon_{xy}\}^T \end{aligned} \tag{3}$$

As far as the geometrical relations are concerned, the Green-Lagrange nonlinear strain components are

$$\boldsymbol{\epsilon} = \boldsymbol{\epsilon}_l + \boldsymbol{\epsilon}_{nl} = (\mathbf{b}_l + \mathbf{b}_{nl})\mathbf{u}, \tag{4}$$

The 6×3 $\mathbf{b}_l$ and $\mathbf{b}_{nl}$ matrices are the linear and nonlinear differential operators as defined in [5]. As far as the constitutive relation is concerned, linear elastic metallic shell structures are considered in this work. Consequently, the constitutive relation reads as:

$$\boldsymbol{\sigma} = \mathbf{C}\boldsymbol{\epsilon} \tag{5}$$

where C is the material elastic matrix, whose explicit form can be found in many books, see [6, 7]. Finally, introducing the CUF and FEM relations into Eq. (4), the strain vector can be written in algebraic form as follows:

$$\boldsymbol{\epsilon} = (\mathbf{B}_l^{\tau i} + \mathbf{B}_{nl}^{\tau i})\mathbf{q}_{\tau i} \tag{6}$$

where $\mathbf{B}_l^{sj}$ and $\mathbf{B}_{nl}^{sj}$ are the linear and nonlinear algebraic matrices with CUF and FEM formulations. The explicit form of these two matrices is not reported here for the sake of brevity, but they are reported in [5].

3 Nonlinear free vibration

This section provides a brief introduction to vibration analysis. The principle of virtual displacements is employed to derive the nonlinear governing equations, stating that the virtual variation of the internal strain energy and inertial forces is equal to the virtual variation of the external forces.

$$\mathbf{K}_S^{ij\tau s}\ \mathbf{q}_{\tau i} = \mathbf{p}_{sj} \tag{7}$$

Here, $\mathbf{K}_S^{ij\tau s}$ and $\mathbf{p}_{sj}$ represent the FNs of the secant stiffness matrix and the vector of nodal loadings, respectively. These equations are solved using the Newton–Raphson method with the arc-length approach [8, 9]. Similarly, the FNs of the mass matrix are derived from the virtual variation of the inertial loads:

$$\delta L_{\text{int}} = \delta \mathbf{q}_{sj}^T \mathbf{M}^{ij\tau s} \ddot{\mathbf{q}}_{\tau i} \tag{8}$$

in which $\mathbf{M}^{ij\tau s}$ represents the FN of the mass matrix and $\ddot{\mathbf{q}}_{\tau i}$ indicates the nodal acceleration vector; the dot stands for time derivative. As the modal behavior of a structure is not solely determined by its geometric and mechanical characteristics but is inherently tied to the state of equilibrium, eigenfrequencies and eigenmodes may experience sudden aberrations in deep nonlinear regimes [10]. To explore this aspect, vibration analysis is conducted around a linearized equilibrium state along the nonlinear path. Through the linearization of the virtual variation of the nonlinear strain energy, the tangent stiffness matrix ($\mathbf{K}_T$) is introduced.

$$\begin{aligned}
&\delta(\delta L_{\text{int}} + \delta L_{\text{ine}} - \delta L_{\text{ext}}) \\
&\delta \mathbf{q}_{sj}^T (\mathbf{K}_0^{ij\tau s} + \mathbf{K}_{T1}^{ij\tau s}) \mathbf{q}_{\tau i} + \delta \mathbf{q}_{sj}^T \mathbf{K}_\sigma^{ij\tau s} \mathbf{q}_{\tau i} + \delta \mathbf{q}_{sj}^T \mathbf{M}^{ij\tau s} \ddot{\mathbf{q}}_{\tau i} \\
&\delta \mathbf{q}_{sj}^T \mathbf{K}_T^{ij\tau s} \mathbf{q}_{\tau i} + \delta \mathbf{q}_{sj}^T \mathbf{M}^{ij\tau s} \ddot{\mathbf{q}}_{\tau i} = 0
\end{aligned} \tag{9}$$

In deriving Eq. (9), it is assumed that the mass matrix is linear, and $\delta^2 L_{\text{ext}} = 0$ (loading is conservative). Here, $\mathbf{K}_T^{ij\tau s}$ represents the FN of the tangent stiffness matrix, $\mathbf{K}_0^{ij\tau s}$ indicates the linear component of $\mathbf{K}_T^{ij\tau s}$, $\mathbf{K}_{T1}^{ij\tau s} = 2\,\mathbf{K}_{lnl}^{ij\tau s} + \mathbf{K}_{nll}^{ij\tau s} + 2\,\mathbf{K}_{nlnl}^{ij\tau s}$ denotes the nonlinear contribution, and $\mathbf{K}_\sigma^{ij\tau s}$ is the geometric stiffness, a function of the linear ($\mathbf{K}_\sigma l^{ij\tau s}$) and nonlinear ($\mathbf{K}_{\sigma_{nl}}^{ij\tau s}$) pre-stress state, where:

$$\sigma = \sigma_l + \sigma_{nl} = \mathbf{C}(\epsilon_l + \epsilon_{nl}) \tag{10}$$

Finally, the full global stiffness matrices are obtained by assembling the FNs versus the indexes τ, s = 1, ..., M and i, j = 1, ..., $p + 1$. For more details about the expansion of the FNs and the finite element assembly procedure in the framework of CUF, the readers are referred to Carrera *et al.* [2].

The displacement variations in Eq. (9) are considered small, allowing for the assumption of harmonic vibration. Consequently, the system can be solved as a linear eigenvalue problem. In summary, vibrations around nonlinear equilibrium states can be conducted as follows:

- Initially, the static geometrical nonlinear problem is resolved using the Newton–Raphson method based on the arc-length approach.

- Subsequently, after computing the nonlinear equilibrium curve, the tangent stiffness matrix is determined at each state of interest.
- Following this, by taking into account the incremental linearized equilibrium condition of Eq. (9) and assuming harmonic motion around nontrivial equilibrium states,

$$\begin{aligned} \delta\mathbf{q}_{\tau i}(t) &= \delta\tilde{\mathbf{q}}_{\tau i}e^{i\omega t} \\ \delta\ddot{\mathbf{q}}_{\tau i}(t) &= -\omega^2\delta\tilde{\mathbf{q}}_{\tau i}e^{i\omega t} \end{aligned} \tag{11}$$

  The equations of motion are simplified into a linear eigenvalue problem, allowing the evaluation of natural frequencies and mode shapes:

$$(\mathbf{K}_T^{ij\tau s} - \omega^2\mathbf{M}^{ij\tau s})\tilde{\mathbf{q}}_{\tau i}e^{i\omega t} = 0 \tag{12}$$

  Here, ω represents the natural frequency, and $\tilde{\mathbf{q}}_{\tau i}$ is the eigenvector. Additionally, for clarity, it is crucial to emphasize that the nonlinear vibrations exhibit low amplitudes, and small increments of amplitudes are considered when determining the nonlinear vibration modes. Consequently, it is legitimate to employ linearization around the state of equilibrium for problem resolution.

Usually, a resolution based on a linear approach is standard in most literature. Therefore, this work emphasizes the comparison between linear and nonlinear approaches, highlighting the necessity of adopting a complete nonlinear formulation for accurate analyses. Through linearization around the trivial equilibrium state, the tangent stiffness matrix is expressed as:

$$\mathbf{K}_T = \mathbf{K}_0 + \lambda\mathbf{K}_{\sigma l} \tag{13}$$

Here, λ represents the progressively increasing load factor. This simplified linearized approach is executed by substituting Eq. (13) into Eq. (9), wherein $\mathbf{K}_{T1}$ tends to zero due to the small values of δu.

4 Numerical results

The results of numerical analyses performed on thin structures composed of repeatable cells are reported in this section The geometry of the structures is reproduced following the data reported in [13]; in the present case, the structure is composed of repeatable cells having the same dimensions, as shown in Fig. 3. A modal analysis performed by means of the proposed numerical model outlined in Section 2 is discussed; namely, the natural frequencies and the evolution of the band gap is commented on when varying the traction load P.

4.1 Single-cell structure

The first case involves the one-cell structure shown in Fig. 3. The nonlinear equilibrium curve, depicting the response to a traction force P, is illustrated in Fig. 4, along with selected fully nonlinear deformed configurations. The assessment also includes the examination

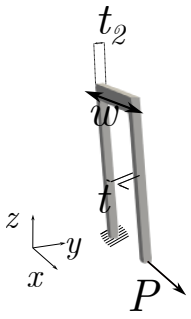

Figure 3: Analyzed structures with repeatable cells. t = 10mm and w = 100 mm.

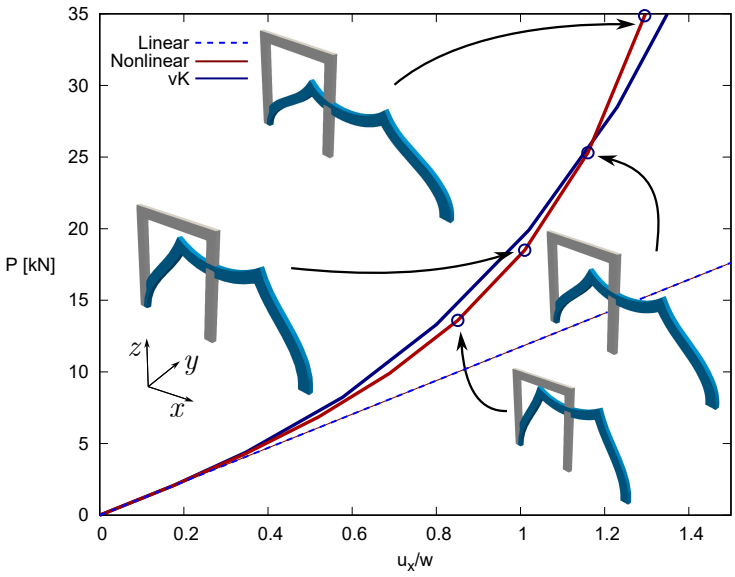

Figure 4: Linear and nonlinear static curve of the one-cell structure. *Nonlinear* curve is evaluated using the full Green-Lagrange strain tensor, *vK* with the von Kármán nonlinearities. Depicted deformed configurations are at nonlinear equilibrium states.

of the curve with von Kármán nonlinearities (refer to [12] for details on modeling von Kármán nonlinearities within the CUF framework). Clear distinctions are observable among the three curves, encompassing variations between the complete nonlinear curve and those incorporating von Kármán nonlinearities. Those distinctions are more evident in Fig. 5, where the mode evaluation between the full nonlinear and the von Kármán solutions are presented. Therefore,

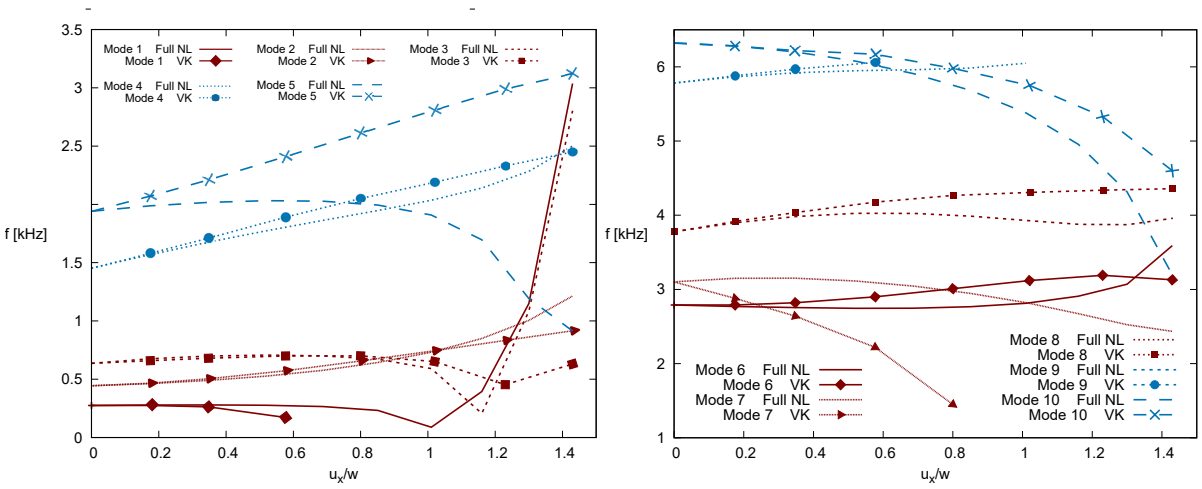

(a) (b)

Figure 5: Mode evolution of the one-cell structure, using full nonlinear (Full NL) and von Kármán (VK) solutions.

employing the complete nonlinear matrix is essential and will be used for all subsequent analyses, referred to as the *nonlinear* configuration.

The natural frequencies are assessed at various equilibrium states. This process is carried out for both linear and nonlinear solutions, with the corresponding outcomes presented in Fig. 6. The first ten frequencies are computed, and in Fig. 6, each curve corresponds to a distinct mode shape. Four distinct band gaps are evident from the mode distribution, and each is individually examined, comparing the linear and nonlinear solutions. Focusing on the first band gap, detailed in Fig. 7, three values of u_x/w (0.69, 0.85, and 1.01) are considered. In the linear solution, the band gap diminishes as u_x/w increases, disappearing entirely at $u_x/w = 1.01$. In the nonlinear domain, the band gap is situated between modes 3 and 4 for $u_x/w = 0.69$and 0.85 while it shifts to modes 2 and 5 for $u_x/w = 1.01$. This shift results from mode alterations and aberrations in the nonlinear field. The corresponding mode shapes in the nonlinear field are presented in the same figure.

The frequencies corresponding to the previously examined band gap are provided in Table 1. The substantial difference in range between the linear and nonlinear solutions is significant and cannot be overlooked. Consequently, it is imperative to incorporate the nonlinear stiffness matrix in the assessment of band gaps within the large displacement field.

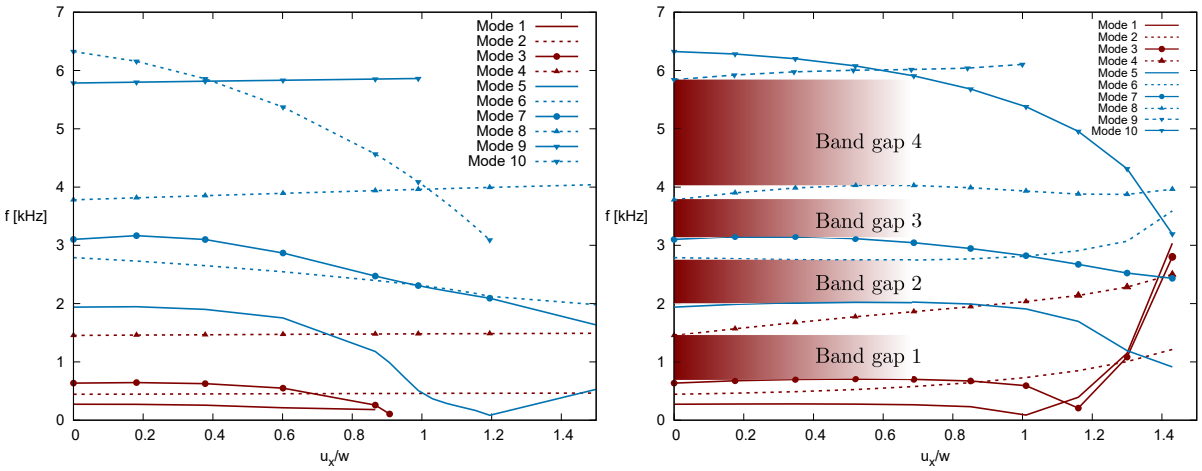

Figure 6: Mode evolution of the one-cell structure, using linear (a) and nonlinear (b) stiffness matrix.

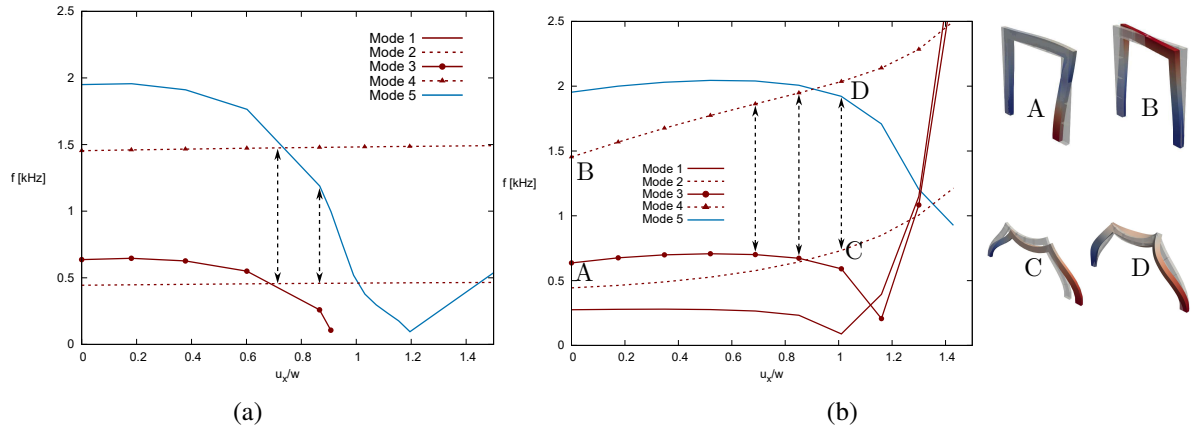

Figure 7: First band gap evolution with linear (a) and nonlinear (b) stiffness matrix. One-cell structure case.

Band gap	u_x/w	$f_{1_{lin}}^{n\ mode}$ - $f_{2_{lin}}^{n\ mode}$	$f_{1_{nl}}^{n\ mode}$ - $f_{2_{nl}}^{n\ mode}$	% range diff.
	0.69	0.454^3 - 1.479^4	0.700^3 - 1.863^4	12%
1 Fig. 7	0.85	0.458^3 - 1.179^4	0.672^3 - 1.947^4	43%
	1.01	—	0.732^2 - 1.909^5	—

Table 1: Values of frequency limits of the one-cell structure case band gaps. Frequencies expressed in [kHz]. f_{lin} stands for frequency evaluated using linear stiffness matrix, f_{nl} using nonlinear stiffness matrix. % range diff. is the percentage difference between the band gaps evaluated using linear and nonlinear stiffness matrix.

4.2 Multi-cell structure

This section proposed the results of the band gap evaluation of multi-cell structure with five cells of the same geometry shown in Fig. 3. Figure 8 shows the linear and nonlinear static behavior of this structure. The deformed configuration at $u_x = 3.2$ is reported in the same

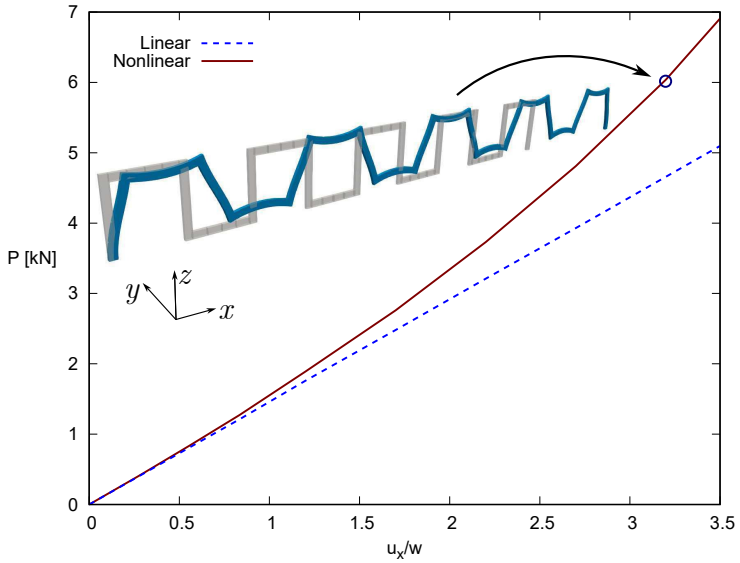

Figure 8: Linear and nonlinear static curve of the five-cell structure. Depicted deformed configurations are at nonlinear equilibrium states.

figure. Figure 9 reports the mode change of such structure, including the first six modes using a full nonlinear approach. The band gap between modes 3 and 6 is analyzed hereafter and the related frequency values are reported in Table 2. Clearly, this band gap arises from both linear and nonlinear solutions for $u_x = 2.2, 2.7$ and 3.2, and it remains between modes 3 and 6. However, as underlined by Table 2, the % difference between the two band gaps is high, especially in the far nonlinear regime, reaching values of 51% and 47% for $u_x = 2.2$ and 2.7, respectively.

Band gap	u_x/w	$f_{1_{lin}}^{n\ mode}$ - $f_{2_{lin}}^{n\ mode}$	$f_{1_{nl}}^{n\ mode}$ - $f_{2_{nl}}^{n\ mode}$	% range diff.
Fig. 9	1.70	0.103^3 - 0.145^6	0.133^3 - 0.168^6	-20%
	2.20	0.097^3 - 0.123^6	0.124^3 - 0.177^6	51%
	2.70	0.082^3 - 0.111^6	0.113^3 - 0.184^6	47%

Table 2: Values of frequency limits of the five-cell structure case band gaps. Frequencies expressed in [kHz]. f_{lin} stands for frequency evaluated using linear stiffness matrix, f_{nl} using nonlinear stiffness matrix. % range diff. is the percentage difference between the band gaps evaluated using linear and nonlinear stiffness matrix.

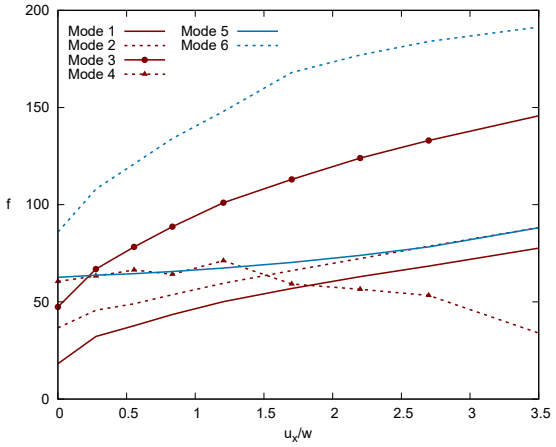

Figure 9: Mode trend of the multi-cell structure, using nonlinear stiffness matrix.

4.3 Multi-cell structure with different material

In contrast to the previous study case, where the structure was made entirely of aluminum, this study evaluates the natural frequencies and mode evolution for a multi-cell repeatable structure composed of alternating aluminum and titanium components, as shown in Fig. 10. This

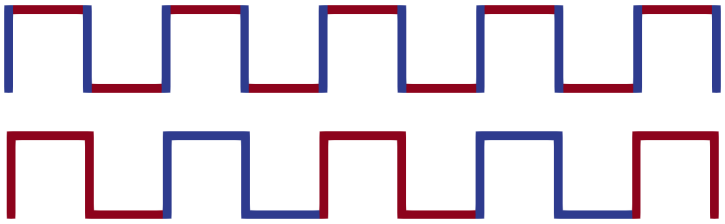

Figure 10: Materials considered for the multiple-cell structure: blue = aluminium, red = titanium.

investigation aims to preliminarily assess the influence of the material properties on the dynamic characteristics, natural frequencies, and band gap evolution under various equilibrium conditions. The materials used in these analyses have the following properties: an elastic modulus of 75 GPa and 116 GPa, and a density of 2700 kg/m^3 and 4500 kg/m^3 as aluminum and titanium alloys, respectively. The two configurations shown in Fig. 9 will be referred to as 'ABAB' and 'AABB' in the subsequent analyses. The static curves, both linear and nonlinear, are reported in Fig. 11. Figure 12 shows the results of the trend of the natural frequencies as the equilibrium condition changes, i.e. as the load P increases, for the ABAB configuration; the x-axis reports the axial displacement u of the force application point, normalized by the cell characteristic length w. It can be observed that the use of a different combination of materials for the considered thin-walled structure introduces an alteration of the natural frequencies, and consequently of the band gap. Moreover, using a material with increased elastic modulus and

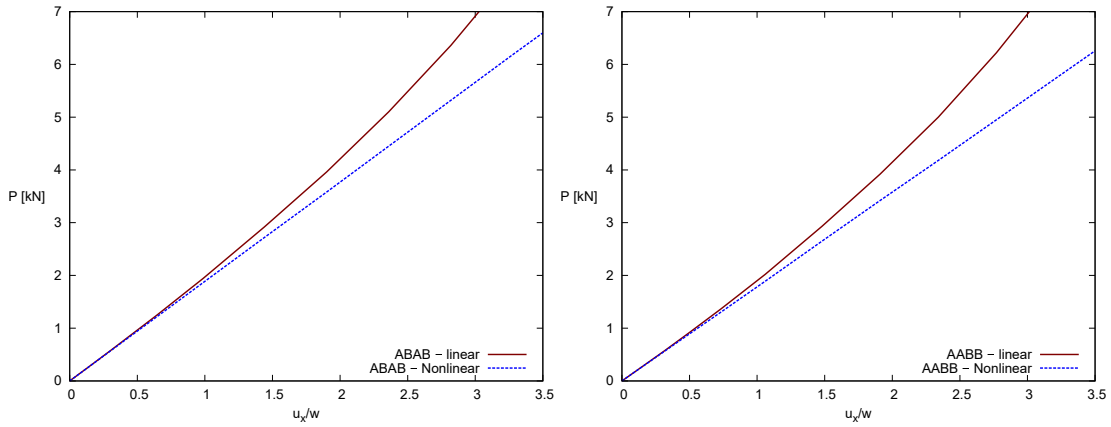

Figure 11: Static linear and nonlinear curves for ABAB and AABB configurations.

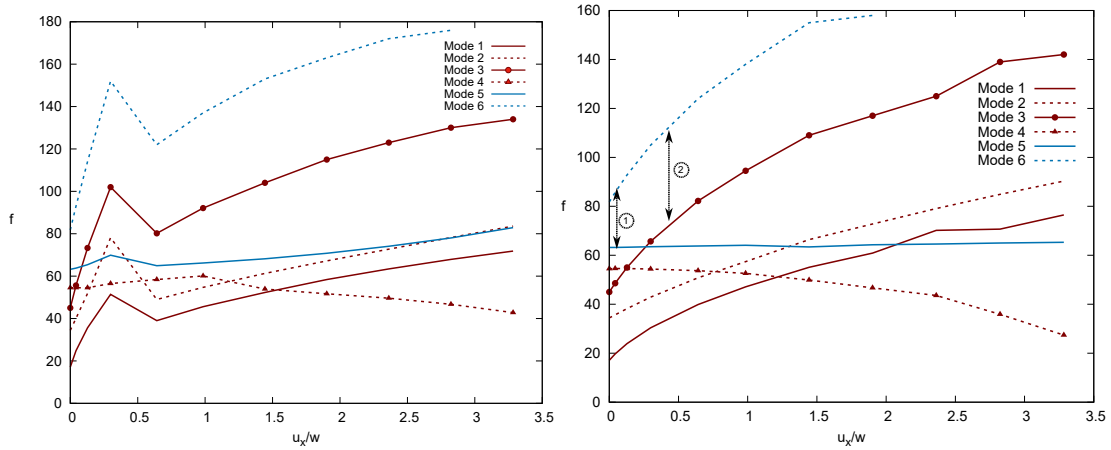

Figure 12: Mode and band-gap evolution for the ABAB configuration. Linear and nonlinear solutions.

density, as the titanium, leads to an increase in stiffness and mass of the structure; in this specific case, the second effect has a larger prevalence, consequently leading to a decrease of the natural frequencies compared to the aluminum case (Fig. 9). As discussed in [13], an evolution of the band gap is observed as the load increases, highlighting that the natural frequencies are a inherent property of the equilibrium. It is observed that the band gap between the sixth and fifth modes changes substantially as the axial deformation, and hence the load, increases. In particular, considering the notation of Fig. 12, at point 1 the band gap is the smallest, and identifies a frequency difference between mode 5 and mode 6. As the load increases, the gap increases, up to point 2 where there is a switch between mode 5 and mode 3. The same conclusions could be drawn by analyzing the dynamic characteristcs shown in Fig. 13, which shows the mode evolution of the AABB configuration.

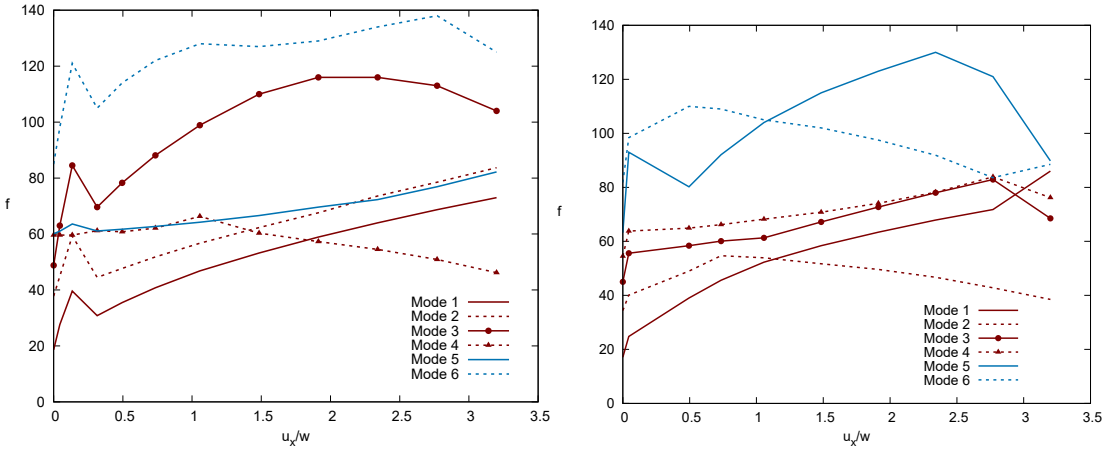

Figure 13: Mode and band-gap evolution for the AABB configuration. Linear and nonlinear solutions.

5 Conclusions

This study explored the dynamic behavior of metamaterials, specifically examining the evolution of their band gaps within the context of large displacements and rotations. The research utilized a unified model based on the Carrera Unified Formulation (CUF), which enabled the development of higher-order one-dimensional beam theories. These theories account for geometric nonlinearities through cross-sectional expansion functions, while the axis was discretized using a finite element approximation. The equations of motion were solved around nonlinear static equilibrium states in a total Lagrangian scenario, identified using a Newton-Raphson algorithm combined with an arc-length path-following method.

The paper provided a detailed comparison of results obtained with both linear and nonlinear stiffness matrices, highlighting the differences between them. Numerical investigations focused on thin-walled structures composed of repeatable cells, assessing mode changes under traction and compression loading conditions. The results clearly indicated that adopting the full Green-Lagrange strain tensor is essential. Additionally, the study introduced a more complex

metamaterial-like structure. The findings emphasized that the band gap is inherently a property of the equilibrium state, underscoring the need for a thorough nonlinear analysis to accurately evaluate frequency transitions.

REFERENCES

[1] E. Carrera, G. Giunta, and M. Petrolo. *Beam structures: classical and advanced theories*. John Wiley & Sons, 2011.

[2] E. Carrera, M. Cinefra, M. Petrolo, and E. Zappino. *Finite element analysis of structures through unified formulation*. John Wiley & Sons, 2014.

[3] E. Carrera and M. Petrolo. Refined beam elements with only displacement variables and plate/shell capabilities. *Meccanica*, 47:537–556, 2012.

[4] A. G. De Miguel, I. Kaleel, M. H. Nagaraj, A. Pagani, M. Petrolo, and E. Carrera. Accurate evaluation of failure indices of composite layered structures via various fe models. *Composites Science and Technology*, 167:174–189, 2018.

[5] A. Pagani and E. Carrera. Unified formulation of geometrically nonlinear refined beam theories. *Mechanics of Advanced Materials and Structures*, 25(1):15–31, 2018.

[6] K.-J. Bathe. *Finite element procedures*. Klaus-Jurgen Bathe, 2006.

[7] T. J. R. Hughes. *The finite element method: linear static and dynamic finite element analysis*. Courier Corporation, 2012.

[8] M. Crisfield. An arc-length method including line searches and accelerations. *International Journal for Numerical Methods in Engineering*, 19(9):1269–1289, 1983.

[9] E. Carrera. A study on arc-length-type methods and their operation failures illustrated by a simple model. *Computers & Structures*, 50(2):217–229, 1994.

[10] G. Kerschen. *Modal analysis of nonlinear mechanical systems*, volume 555. Springer, 2014.

[11] E. Carrera, A. Pagani, D. Giusa, and R. Augello. Nonlinear analysis of thin-walled beams with highly deformable sections. *International Journal of Non-Linear Mechanics*, 128:103613, 2021.

[12] A. Pagani, E. Carrera, and R. Augello. Evaluation of various geometrical nonlinearities in the response of beams and shells. *AIAA Journal*, 57(8):3524–3533, 2019.

[13] R. Augello, and E. Carrera. Nonlinear dynamics and band gap evolution of thin-walled metamaterial-like structures. *Journal of Sound and Vibration* 118329,2024.